THE JOURNAL OF PHYSICAL CHEMISTRY C
A JOURNAL OF THE AMERICAN CHEMICAL SOCIETY

pubs.acs.org/JPCC
Article

SERS Spectra Indicate the Molecular Effects of 7-Nitrobenz-2-oxa-1,3-diazole (NBD) on Living Cells

Published as part of The Journal of Physical Chemistry C special issue "Celebrating 50 Years of Surface-Enhanced Spectroscopy."

Yiqing Feng, Florian Gärber, Essa M. Saied, Cecilia Spedalieri, Zdravko Kochovski, Stephan Werner, Christoph Pratsch, Christoph Arenz, Stephan Seifert, and Janina Kneipp*

Cite This: J. Phys. Chem. C 2024, 128, 19722−19735

Read Online

ACCESS | Metrics & More | Article Recommendations | Supporting Information

ABSTRACT: 7-Nitrobenz-2-oxa-1,3-diazole (NBD) is a widely used fluorescent label for proteins, peptides, and lipids. Its chloride derivative, NBD-Cl, can be highly reactive toward thiol and amine groups, forming stable fluorescent adducts. When labeling the ubiquitous lipid molecule ceramide, NBD-ceramide (NBDCER) aids in visualizing sphingolipid metabolism in cells. This study investigates intracellular molecular changes induced by NBD-Cl and NBDCER using surface-enhanced Raman scattering (SERS). SERS spectra from the endolysosomal compartment of two cell lines, 3T3 fibroblast cells and J774 macrophage cells, obtained with gold nanoparticles as probes, reveal changes in the molecular composition and interactions under different incubation conditions. Applying the random forest (RF)-based algorithm surrogate minimal depth (SMD) to the SERS data to identify important spectral classifiers and their relations, both NBD-Cl and NBDCER are found to alter the biochemical makeup of the endolysosomal compartment. The data indicate significant structural and interaction changes in the molecular constituents of the cells that are in agreement with possible interference of the labels in the cellular metabolism and the reaction of NBD-Cl with functional groups of cellular molecules.

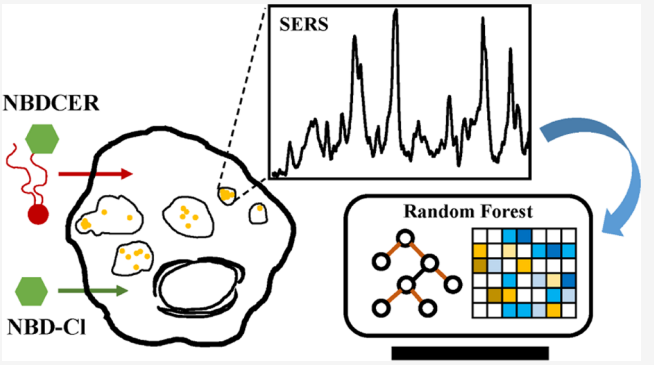

INTRODUCTION

7-Nitrobenz-2-oxa-1,3-diazole (NBD) has been widely used as a fluorescent label for proteins, peptides, and lipids for decades.[1−4] As it is a small neutral chromophore, cell permeability for the molecule is high, and the native properties of labeled biomolecules are retained, making it a powerful labeling tag in biochemical research.[5,6] Its chloride derivative, NBD-Cl (Figure S1A), demonstrates high reactivity with thiol and amine groups based on nucleophilic substitution reactions that lead to stable fluorescent adducts.[1,7] It has been employed in various applications, including tracking protein modifications and monitoring enzyme activities.[8−11] Building on the utility of NBD-Cl, NBD-labeled lipids have helped to substantially advance membrane and cell biological studies.[12] A popular lipid analogue is NBD-ceramide (NBDCER, Figure S1B), combining NBD with a ubiquitous lipid molecule that is a crucial structural component and potent regulator in the physiological responses of eukaryotic cells.[13] NBDCER is extensively used to visualize the uptake and distribution of ceramide by fluorescence microscopy, facilitating studies of sphingolipid metabolism.[2,14,15]

In living cells, NBD-Cl, due to its high reactivity resulting from electron-withdrawing groups, can interact with different types of biomolecules and is expected to act without a specific intracellular location. NBDCER, which is inert and not known to alter other biomolecules inside a cell, tends to accumulate in the Golgi apparatus and may induce apoptosis-like metabolic changes when present in excessive amounts, considering that the cellular metabolism of ceramide itself is not affected by the NBD group.[2,13,15] Here, we analyze the molecular alterations when NBD is introduced into cells in two forms, as NBD-Cl and as NBDCER. We employ surface-enhanced Raman scattering (SERS) that can provide information on molecular composition, structure, and interaction from selected substructures in complex biosamples, such as organelles in living cells.[16] SERS spectra of the endolysosomal compartment and

Received: August 4, 2024
Revised: October 4, 2024
Accepted: October 30, 2024
Published: November 11, 2024

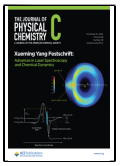

https://doi.org/10.1021/acs.jpcc.4c05260
J. Phys. Chem. C 2024, 128, 19722−19735

intracellular vacuoles have helped to characterize the molecular composition and interaction in these compartments in different conditions, including apoptosis and the inhibition of enzymes by drugs.[17] SERS can reveal spectral signals of molecules of low abundance and/or low Raman cross sections and their structure, including lipids, under nonresonant conditions and without the use of additional labels, and is restricted to the local environment of metal nanostructures, enabling the probing of very confined regions in a cell.[18−20] Due to the involvement of the endolysosomal compartment in important metabolic pathways in healthy cells as well as in apoptotic events, we collected SERS spectra from the endolysosomes of cells treated with NBD-Cl and NBDCER with gold nanoparticles (AuNPs) that serve as SERS probes.

While the structure and interaction of lipids, proteins, drugs, or other molecules when they are present as pure substances can be inferred from their SERS spectra,[18] their spectral characterization in mixtures or the complex biomatrix requires experiments with suitable models as well as data evaluation strategies that take into account the great variation of SERS data regarding absolute and relative signal strengths that depend on a multitude of different factors.[16] We have shown previously that the random forest (RF)-based algorithm surrogate minimal depth (SMD)[21] can help to retrieve the vibrational information on biomolecular structure and interaction in drug-induced enzyme inhibition that affected lipid processing in the endolysosomal compartment of living cells.[17,22]

SMD has been developed to select relevant features by an evaluation of their mutual impact on random forest models.[21] It can also be used to quantify the relationship between variables. The selection and relation analysis of SMD allows for a comprehensive detection of correlations that are responsible for a particular classification and regression obtained by RF.[23−28] In an analysis of SERS data, SMD enables the selection of co-occurring spectral signals and thereby can reveal biomolecular interactions.[29]

Here, we apply RF analysis based on SMD to identify differences in molecular composition and interactions that can be related to exposure of cells from two different cell lines to external NBD-Cl and NBDCER. As will be discussed, the spectra clearly show that both forms of NBD labels affect the biochemical composition in the endolysosomal compartment of the living cells and that the effects vary for the cell lines and for the type of NBD label.

EXPERIMENTAL SECTION

Preparation of Gold Nanoparticles and Lipid Nanoparticle Samples. Gold(III) chloride hydrate, sodium citrate dehydrate, ceramide, NBD-Cl, phosphatidic acid, and phosphatidylcholine were purchased from Sigma-Aldrich (Steinheim, Germany). 30 nm of citrate-stabilized gold nanoparticles were synthesized by the protocol described in ref 30 from solutions prepared using Milli-Q ultrapure water. NBDCER was synthesized as described in ref 31. Pure ceramide and NBDCER-containing liposome samples were prepared by thin layer hydration, as described previously.[18,19] The NBDCER-containing liposome samples were composed of 10 mol % NBDCER, 10 mol % phosphatidic acid, and 80 mol % phosphatidylcholine in a total concentration of 2 mM. They were rehydrated by gold nanoparticle solution and water in the case of fluorescence experiments, respectively.

Cell Culture and Sample Preparation. Two cell lines, Swiss albino mouse fibroblast cell line 3T3 and macrophage cell line J774 (both from DSMZ, Braunschweig, Germany), were cultured in Dulbecco's modified Eagle's medium (DMEM, Bio&SELL, Nürnberg, Germany) supplemented with 10% fetal calf serum (FCS, Biochrom, Berlin, Germany) under standard conditions (37 °C, 5% CO_2).

For SERS experiments, after cells were grown on glass coverslips for 24 h, the culture medium was exchanged with a dilution of gold nanoparticles in DMEM-FCS of 1:10 (nanoparticle concentration $\sim 10^{-11}$ M). After incubation with the SERS nanoprobes for either 3 or 24 h, the cells were rinsed with phosphate-buffered saline (PBS) (Bio&SELL, Nürnberg, Germany) to remove excess gold nanoparticles before incubation with the NBD labels. Then, the culture medium was exchanged with DMEM-FCS containing 5 μM NBDCER. Following a protocol reported to ensure diffusion through the membrane outer leaflet, the cells were incubated at 4 °C for 30 min, then rinsed with PBS and grown in fresh DMEM-FCS at 37 °C for 15 min.[15] For incubation with NBD-Cl, cells were incubated with 5 μM NBD-Cl in DMEM-FCS at 37 °C for 20 min. Control samples were incubated only with gold nanoparticles. SERS spectra from the cells were measured in PBS after being rinsed with PBS three times.

For cryo-soft X-ray nanotomography (SXT), cells were grown on Formvar-coated gold grids (Quantifoil, Jena, Germany) and incubated as described above. After the incubation, each grid was rinsed three times with PBS, the excess buffer was blotted with filter paper, and the grids were plunge-frozen in liquid ethane.

For comparison by fluorescence microscopy, the cells were incubated with 5 μM NBDCER in DMEM-FCS following the same workflow as described for the SERS experiments but without prior incubation with gold nanoparticles. Then cells were rinsed three times with PBS and during the experiment were kept in PBS.

SERS Experiments. Raman spectra were obtained by excitation with a 785 nm diode laser (Toptica, Munich, Germany) by using a single-stage spectrograph equipped with a CCD detector (Horiba, Munich, Germany). A 10× objective was used to excite and collect spectra in the experiments with liposomes and pure compounds in aqueous colloidal suspensions, resulting in an excitation intensity of 4×10^4 W/cm^2. The measurement of pure CER samples was performed as described in previous work.[18] For the experiments with the living cells, a 60× water immersion objective was applied, resulting in an intensity of 3.5×10^5 W/cm^2 at the sample. All spectra were recorded with an acquisition time of 1 s and at a spectral resolution of ~2 cm^{-1}, considering the full spectral range used from 300 to 1900 cm^{-1}.

Cryo-Soft X-ray Tomography, Cryo-Electron Microscopy, and Fluorescence Imaging. Vitrified cell monolayers with a thickness of approximately 10 μm were examined using a transmission X-ray microscope equipped with a cryostage at beamline U41-PGM1-XM at the electron storage ring BESSY II (Helmholtz-Zentrum Berlin für Materialien und Energie, Berlin, Germany).[32] Tilt series of individual cells were acquired at different angular ranges in increments of 1° at an image pixel size of 9.8 nm (25 nm zone plate objective) and a photon energy of 510 eV. Depending on the sample thickness, the exposure time was adjusted for each tilt angle series between 1 and 3 s per image. The tilt series consisted of up to 130 images. Tomograms were obtained by alignment of the corrected tilt

https://doi.org/10.1021/acs.jpcc.4c05260
J. Phys. Chem. C 2024, 128, 19722−19735

Table 1. Performance of PLS-DA Models and RF Analysis to Discriminate SERS Spectra from Cells under Two Different Treatments, NBDCER and NBD-Cl

				success rate of identifications			
				PLS-DA		RF	
	SERS probe incubation (h)	NBD label	spectra with signal:full data	training (%)	test (%)	training (%)	test (%)
3T3	3	NBDCER	178:1600	86.62	75	94.37	88.89
		NBD-Cl	162:1800	80	93.75	86.15	84.38
	24	NBDCER	174:800	82.73	94.29	96.40	100
		NBD-Cl	161:2000	86.82	90.62	86.82	68.75
J774	3	NBDCER	84:800	86.57	94.12	100	100
		NBD-Cl	91:800	100	100	97.26	100
	24	NBDCER	53:800	97.62	90.91	95.24	81.82
		NBD-Cl	51:800	95.12	100	95.12	90

series using the intracellular gold nanoparticles as fiducial markers and tomographic reconstruction using Etomo software (IMOD, Colorado). The reconstruction of sample volumes was carried out by back-projection or a simultaneous iterative reconstruction technique.

For cryo-electron microscopy (cryo-EM), 4 μL liposome−nanoparticle suspensions were deposited on lacey carbon-coated copper transmission electron microscopy (TEM) grids (Electron Microscopy Sciences, Hatfield, PA) and then plunge-frozen in liquid ethane with a Vitrobot Mark IV (FEI, Eindhoven, The Netherlands) under 4 °C and 95% humidity. An NBDCER-containing liposome sample with gold nanoparticles was measured by using a JEOL JEM-2100 transmission electron microscope (JEOL GmbH, Eching, Germany). Cryo-EM imaging was carried out at a temperature of around 90 K at an acceleration voltage of 200 kV. A defocus of the objective lens of about 0.5 and 1 μm was used to increase the contrast. Cryo-EM micrographs were recorded at a number of magnifications with a bottom-mounted 4k CMOS camera (TemCam-F416, TVIPS, Gauting, Germany). The total electron dose in each micrograph was kept below 20 $e^-/Å^2$.

Fluorescence images were obtained using an Axioplan 2 Imaging microscope with an LSM 5 Pascal confocal laser-scanning module and an AxioCamHR camera (Carl Zeiss, Jena, Germany). Fluorescence was excited using a 488 nm Ar laser, and emission was detected with an LP 505 nm filter. Images were acquired using Epiplan-Neofluar HD DIC objectives (20× N.A. 0.5; 50× N.A. 0.8; 100× N.A. 0.9) and LSM PASCAL software and further processed using Fiji.[33]

Data Analysis. The SERS spectra were frequency-calibrated using a spectrum of a toluene−acetonitrile mixture (1:1) and preprocessed regarding removal of spikes, baseline correction using asymmetric least-squares (AsLS),[34] and vector-normalization in MatLab R2020b (The MathWorks, Inc., Natick, MA). After the removal of spectra with no signal from the data sets, the remaining spectra (Table 1) in the range of 400−1800 cm^{-1} were subjected to different analyses. The relative occurrence of signals in individual spectra was analyzed using a script in Mathematica 12.1 (Wolfram, Champaign, IL) as detailed in ref 35. Principal component analysis (PCA) was performed with preprocessed individual SERS spectra. Partial Least-Squares Discriminant Analysis (PLS-DA) was done using a Classification toolbox developed by Milano Chemometrics.[36] In each comparison, a discriminate model with 10 latent variables was developed using a randomly selected subset comprising 80% of the spectra as a training data set, and the remaining 20% of the spectra were used as respective test data sets. The model performance was assessed by Venetian blind cross-validation. Average spectra of each class were calculated for the further qualitative analysis of SERS signals.

Random forest analysis was conducted with the same training and test data sets in R 4.2.2[37] using *ranger* 0.15.1[38] and *RFSurrogates* 0.4.0.[21,39] For the training of the RF classification model, the number of trees (*num.trees*) and the number of variables to consider in each split (*mtry*) were set to 10,000 and 160 (corresponding to $p^{3/4}$, where p is the total number of spectral variables), respectively. To select relevant spectral variables and analyze their co-occurrence, surrogate minimal depth (SMD) was applied with the RF parameters described above and a predefined number of surrogate splits (s) of 44, corresponding to 0.05 p. The output of SMD contains the SMD feature importance of each variable—lower values correspond to higher importance— and a list of selected variables that have a lower importance value than the calculated threshold. In addition, the relation parameter mean adjusted agreement (MAA) was obtained for the pairwise combination of features. The relations of the selected variables to each spectral variable were depicted in a heatmap (Supporting Information). One representative variable was determined from all selected variables of each signal by choosing the variable with the lowest SMD importance value (corresponding to the highest importance), and the relations of those variables to all p spectral variables were depicted.

RESULTS AND DISCUSSION

SERS Spectra of Liposomes Containing NBD-Labeled Ceramide. SERS spectra were collected of NBDCER-containing liposomes and of pure NBD-Cl with the help of gold nanoparticles that acted as plasmonic substrates (Figure 1). Similar to liposome samples containing unlabeled ceramide, as reported in ref 18, intact unilamellar and multilamellar vesicles with sizes ranging from ∼25 nm to ∼550 nm were found to form (Supporting Figure S2A,B), showing that liposome formation is not compromised in the presence of the NBD label. The liposomes also show a green fluorescence due to the presence of NBD in the absence and presence of gold nanoparticles (Figure 2A and Supporting Information Figure S2C). The SERS spectra were excited at a wavelength of 785 nm under non(molecular-)resonant conditions with the fluorophore. Figure 1 shows the spectra together with a SERS spectrum of pure ceramide (CER) that we have discussed in earlier work.[18]

The SERS spectrum of liposomes containing NBDCER (Figure 1, middle trace, red) shows characteristic vibrations of

https://doi.org/10.1021/acs.jpcc.4c05260
J. Phys. Chem. C 2024, 128, 19722−19735

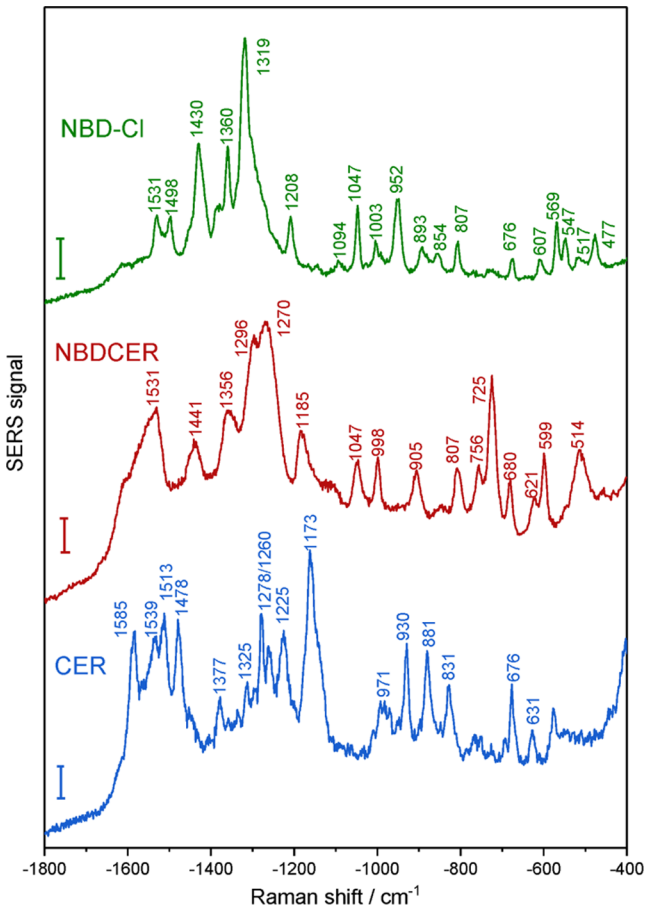

Figure 1. Representative SERS spectra of NBD-Cl (green trace), NBD-ceramide (NBDCER, red trace), and ceramide (CER, blue trace) with gold nanoparticles (c_{AuNP} = 6 × 10^{-10} M). c_{NBD-Cl} = 0.1 mg/mL, c_{NBDCER} = 0.1 mM, c_{CER} = 2 mM; excitation wavelength: 785 nm; excitation intensity: 4 × 10^4 W/cm^2 in NBD-Cl and NBDCER solution, and 3.5 × 10^5 W/cm^2 in CER lipid preparation; acquisition time: 1 s; scale bars: 50 cps.

the amide group, specifically amide II at 1531 cm^{-1}, amide III at 1270 cm^{-1}, and amide IV at 680 cm^{-1}, which is consistent with the spectrum of pure CER (blue line).[18,40,41] It indicates similar interactions of the sphingosine headgroup in the NBD-labeled ceramide NBDCER with AuNPs as those of pure ceramide samples.[18] From the signal characteristic of the intrachain C−C vibration at 1047 cm^{-1} in NBDCER and the chain-end CH_3 rocking vibrations at 881 and 831 cm^{-1} in CER (Figure 1, compare middle and bottom trace),[18,40,42] we infer on different acyl chain conformations in both molecules. The pronounced intrachain C−C signal suggests that when combined with an NBD label, the ceramide acyl chains are more likely to be exposed and to interact with the AuNPs. The absence of the chain-end CH_3 modes in the NBDCER spectrum could also be related to a lower possibility of interactions of the acyl chain-ends with the AuNPs when the NBD group is linked to them (Figure S1B). When comparing the spectrum of NBDCER with that of NBD-Cl (Figure 1, compare middle and top trace), characteristic signals of NBD can be identified in the NBDCER spectrum, including a typical C═N stretching mode at 1356 cm^{-1}, C−C−C two in-plane modes and an out-of-plane bending mode from the benzofurazan ring at 999, 599, and 514 cm^{-1}, an NO asymmetric stretching vibration at 905 cm^{-1} and a band assigned to the NO_2 group attached to the NBD ring at 807 cm^{-1}, respectively.[43,44] The pronounced presence of these modes indicates that the nitro group and the benzofurazan ring of the NBD group interact with the AuNPs. This is also found in NBDCER liposomes, despite the different types of interactions that are possible when ceramide is present.[18]

Fibroblast and Macrophage Cells Display Different SERS Spectra after Treatments with NBD Labels. Scheme 1 displays the incubation sequence that was used to introduce the NBD labels and the SERS probes into cells of two different cell lines. Confocal fluorescence microscopy indicates the uptake of NBDCER by cells of two different cell lines, 3T3 fibroblast (Figure 2B) and J774 macrophage cells (Figure 2C), according to Scheme 1. In both cell types, bright fluorescence is located adjacent to the nuclear region. Especially in 3T3 (Figure 2B), due to the larger size of the cells, both predominant staining at one side of the nucleus and punctate fluorescence above the nuclei are consistent with a gradual redistribution from mitochondria to the Golgi apparatus and later to the plasma membrane, as NBDCER is translocated and metabolized as has been discussed in previous work.[15]

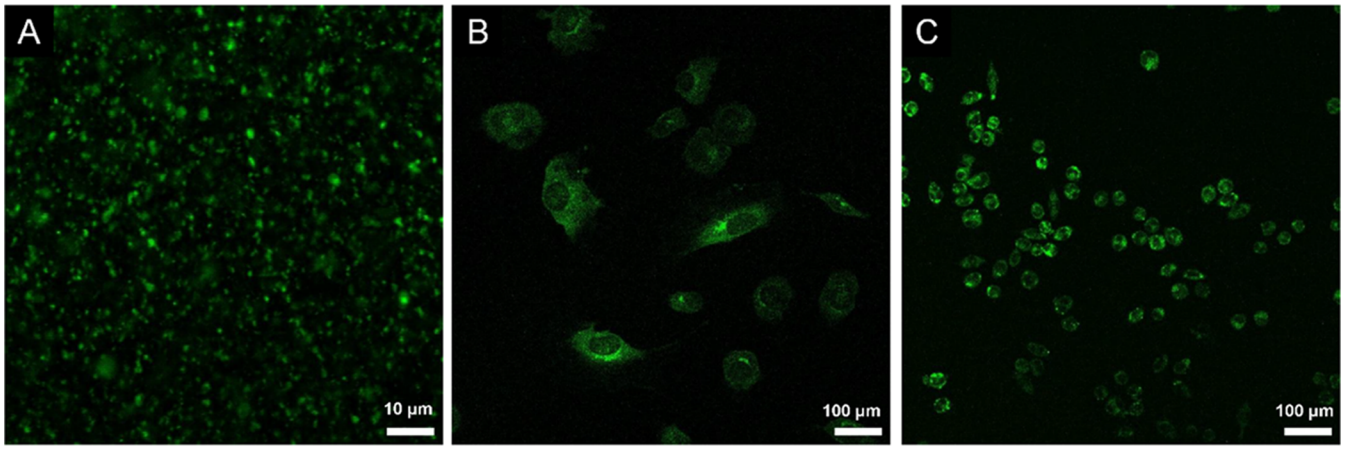

Figure 2. Fluorescence images of (A) liposomes containing NBDCER rehydrated by gold nanoparticles (c_{AuNP} = 6 × 10^{-10} M) and (B) 3T3 cells and (C) J774 cells incubated with 5 μM NBDCER. Liposome composition: 10 mol % NBDCER, 10 mol % phosphatidic acid, and 80 mol % phosphatidylcholine, total lipid concentration: 2 mM. Fluorescence excitation wavelength: 488 nm; filter: LP 505.

https://doi.org/10.1021/acs.jpcc.4c05260
J. Phys. Chem. C 2024, 128, 19722−19735

Scheme 1. Cell Samples Incubated with Gold Nanoparticles, NBDCER, and NBD-Cl for SERS Experiments: Cells Were Incubated with SERS Probe Gold Nanoparticles for 3 or 24 h Prior to the Treatments with NBDCER or NBD-Cl

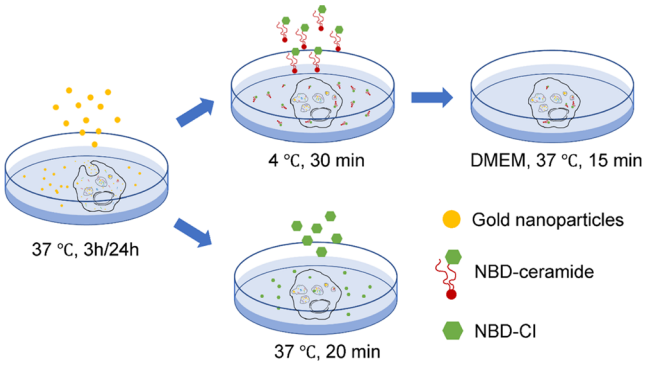

However, when exposed to NBD-Cl, the cells did not exhibit discernible fluorescence signals that could indicate preferential accumulation (data not shown). We conclude that the reactivity of NBD-Cl will lead to its intracellular binding to various types of molecules regardless of their intracellular distribution, so that accumulation of NBD-Cl in specific cellular regions or compartments is lacking, different from that of NBDCER.

As indicated in Scheme 1, both cell types contained gold nanoparticles that function as SERS probes for the endolysosomal compartment after NBDCER or NBD-Cl uptake. Figure 3 shows the results of statistical analyses of SERS signals in the spectra of 3T3 and J774 cells treated with NBDCER (red) and NBD-Cl (green) after the incubation with gold nanoparticles for two different periods of time (cf. Supporting Information Table S1 for a list of all tentative band assignments). Cells that were only incubated with gold nanoparticles and with neither of the NBD labels (Figure 3, bottom row, black) served as controls. Due to varying interactions between gold nanoparticles and biomolecules in complex cellular systems, individual spectra can exhibit great differences regarding overall signal strength and qualitative features under identical conditions, as shown for the example of spectra from 3T3 cells incubated with gold nanoparticles for 3 h in Figure S3. To enable a discussion of the spectral variation independently of such differences,[35] the relative occurrence of specific bands was determined (Figure 3). The total amount of gold nanoparticles in the cells and the number of late-stage endolysosomes are expected to be lower after exposure to gold nanoparticles in the culture medium for 3 h (Figure 3A−C,G−I) compared to incubation for 24 h (Figure 3D−F,3J−L), as shown for both cell types in previous work.[45,46] All samples show several common spectral features that include characteristic vibrational modes of proteins, specifically a band of tryptophan (Trp) at ∼1350 cm^{-1}, a

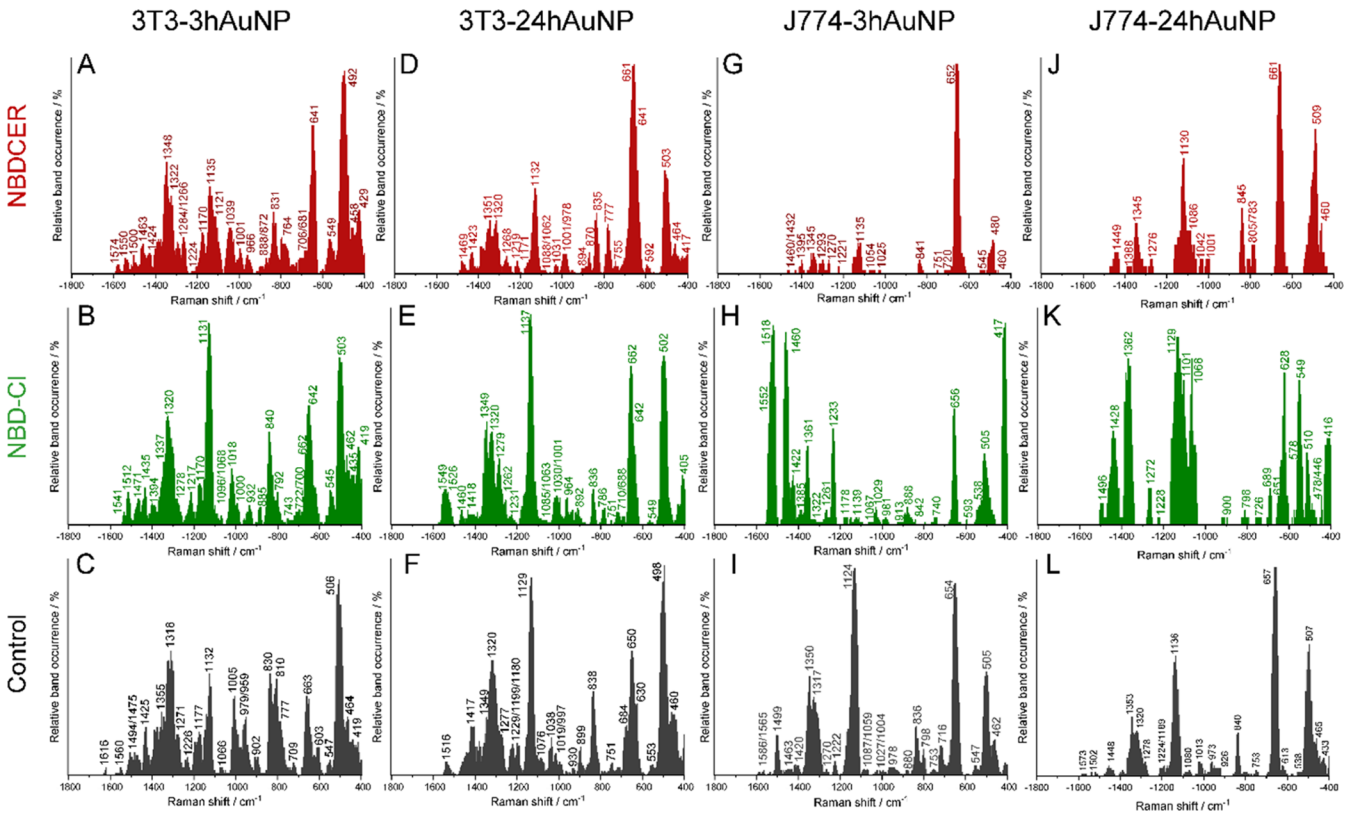

Figure 3. Relative band occurrence of the respective SERS data sets of (A, D) 3T3 cells incubated with NBDCER, (B, E) NBD-Cl after incubation with gold nanoparticles for (A, B) 3 h and (D, E) 24 h and control samples incubated only with gold nanoparticles for (C) 3 h and (F) 24 h, and (G, J) J774 cells incubated with NBDCER, and (H, K) NBD-Cl after incubation with gold nanoparticles for (G, H) 3 h and (J, K) 24 h and gold nanoparticles for (I) 3 h and (L) 24 h. Each data set contains 178 (A), 162 (B), 193 (C), 174 (D), 161 (E), 296 (F), 84 (G), 91 (H), 181 (I), 53 (J), 51 (K), and 150 (L) SERS spectra, respectively, after elimination of spectra with no signal after the experiment. Excitation wavelength: 785 nm. Excitation intensity: 3.5×10^5 W cm^{-2}. Acquisition time: 1 s.

https://doi.org/10.1021/acs.jpcc.4c05260
J. Phys. Chem. C 2024, 128, 19722−19735

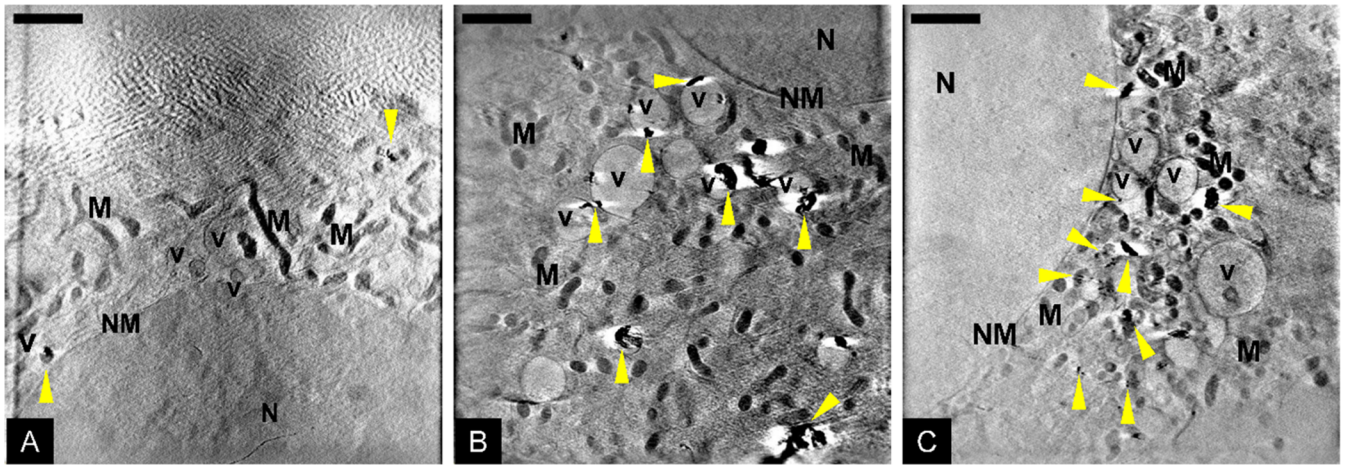

Figure 4. Tomographic slices of 3T3 cells incubated with (A) AuNPs for 24 h (the control), (B) 5 μM NBDCER after 24 h incubation of AuNPs, and (C) 5 μM NBD-Cl after 24 h incubation of AuNPs. M: mitochondrion, V: vesicle, NM: nuclear membrane, N: nucleus. Gold nanostructures are marked with yellow arrowheads. Scale bar: 2 μm.

signal assigned to a protein backbone C−C/C−N vibration at ∼1130 cm^{-1}, a ring breathing mode at ∼830 cm^{-1} that can be assigned to tyrosine (Tyr), phenylalanine (Phe), and proline (Pro), and vibrations due to sulfur-containing amino acids at ∼660 and ∼500 cm^{-1} due to a C−S vibration and a disulfide mode, respectively.[17,47−50] These features are consistent with previous observations that AuNPs interact with proteins in the cell culture medium and that the biomolecular corona that forms as a consequence of this interaction is processed in the endolysosomal system.[35,47]

When 3T3 cells were exposed to NBDCER or NBD-Cl after the incubation with SERS probes, bands around 1050−1100, ∼1120 cm^{-1}, in the range 1430−1465 cm^{-1}, and at 430 cm^{-1} are observed (Figure 3A,B,D,E). They can be assigned to skeletal C−C vibrations and different deformation modes of CH_2 groups in lipids and cholesterol esters[17,40,42,50,51] and indicate interactions of the gold nanoparticles with the endolysosomal membrane.[35] When the incubation with AuNPs was extended to 24 h, the spectra of the NBD-treated cells showed fewer contributions from lipid-related SERS signals (Figure 3D,E).

A comparison of the NBD-treated fibroblast cells shows several common differences in the occurrence of signals with their respective controls (compare 3A, 3B with 3C or 3D, 3E with 3F). Most of these can be assigned to vibrations of proteins. In the cells treated with either of the NBD labels, signals of the amide II and amide III spectral regions (1500−1570 and 1220−1280 cm^{-1}, respectively) appear more often in the spectra compared to the controls.[41,47,48,50] Comparing the abundance of amide II vs amide III signals between the NBDCER treated and the NBD-Cl treated cells, the spectra from the latter exhibited more amide II signals and less amide III contributions, while NBDCER treatment resulted in less amide III signals.

Moreover, vibrations of the C−C/C−N protein backbone at ∼1130 cm^{-1} are much more common in the 3T3 cells treated with either of the NBD labels, specifically with NBD-Cl (Figure 3A).[35,47] Also, the interaction of protein side chains, most clearly visible by the signals of the aromatic amino acids with the SERS nanoprobes, varies for the different samples. For example, proximity of Trp to the gold nanoparticles is indicated by different signals assigned to Trp, namely, a vibration at 1348 cm^{-1} in the spectra of 3T3 cells treated with NBDCER (Figure 3A),[17] and another Trp band at 419 cm^{-1} in the samples treated with NBD-Cl (Figure 3B).[35,47,48] The signal of the Phe ring breathing mode at ∼1000 cm^{-1} is observed less frequently in the NBD-treated samples after 3 h of incubation with the SERS probes (compare Figure 3A and B with C).[47,50] The bands in the region 640−660 cm^{-1}, assigned to C−S vibrational modes, appeared more often in the spectra of the NBD-labeled cells,[35,47,49,50] compared to the controls. Particularly, in addition to this, in the cells treated with NBDCER, fewer spectra displayed signals from the band at 500 cm^{-1} assigned to the S−S vibration of the disulfide bond.[17,47−50] These features suggest that NBDCER and NBD-Cl could alter the interactions of AuNPs and surrounding components differently when cells were incubated with the SERS probes longer.

The altered interaction and composition of proteins are related to the observation that the nanoparticle agglomerates in the cells treated with the NBD labels display different spatial arrangements. Slices from the soft X-ray nanotomograms of the 3T3 cells incubated with NBDCER or NBD-Cl as well as from the control group, respectively, after 24 h of incubation with the SERS probes were reconstructed (Figure 4). Across the three experimental groups, AuNP aggregates of irregular outlines (Figure 4A−C, yellow arrows) were observed in the vesicular structures near mitochondria and in the perinuclear region, in agreement with previous work on the endocytotic uptake of SERS probes into different cell types.[45] Spacing between the individual nanoparticles or smaller aggregates indicates loose assemblies of the gold nanoparticles within the agglomerate structures in all samples. In the control cells (Figure 4A), the majority of agglomerates range in size from ∼100 to ∼500 nm, corresponding to approximately 3 to 15 particles. When cells were continuously exposed to NBDCER and NBD-Cl (Figure 4B,C), slightly larger aggregates were found with sizes up to ∼750 nm, corresponding to assemblies of ∼25 particles. In agreement with a continuous incubation of the cells with gold nanoparticles, also endosomal structures of very few nanoparticles are present. Interestingly, the cells treated with NBD-Cl exhibit a greater abundance of such small aggregates and individual nanoparticles between ∼40 and ∼75 nm (Figure 4C) than the other samples. These changes suggest

https://doi.org/10.1021/acs.jpcc.4c05260
J. Phys. Chem. C 2024, 128, 19722−19735

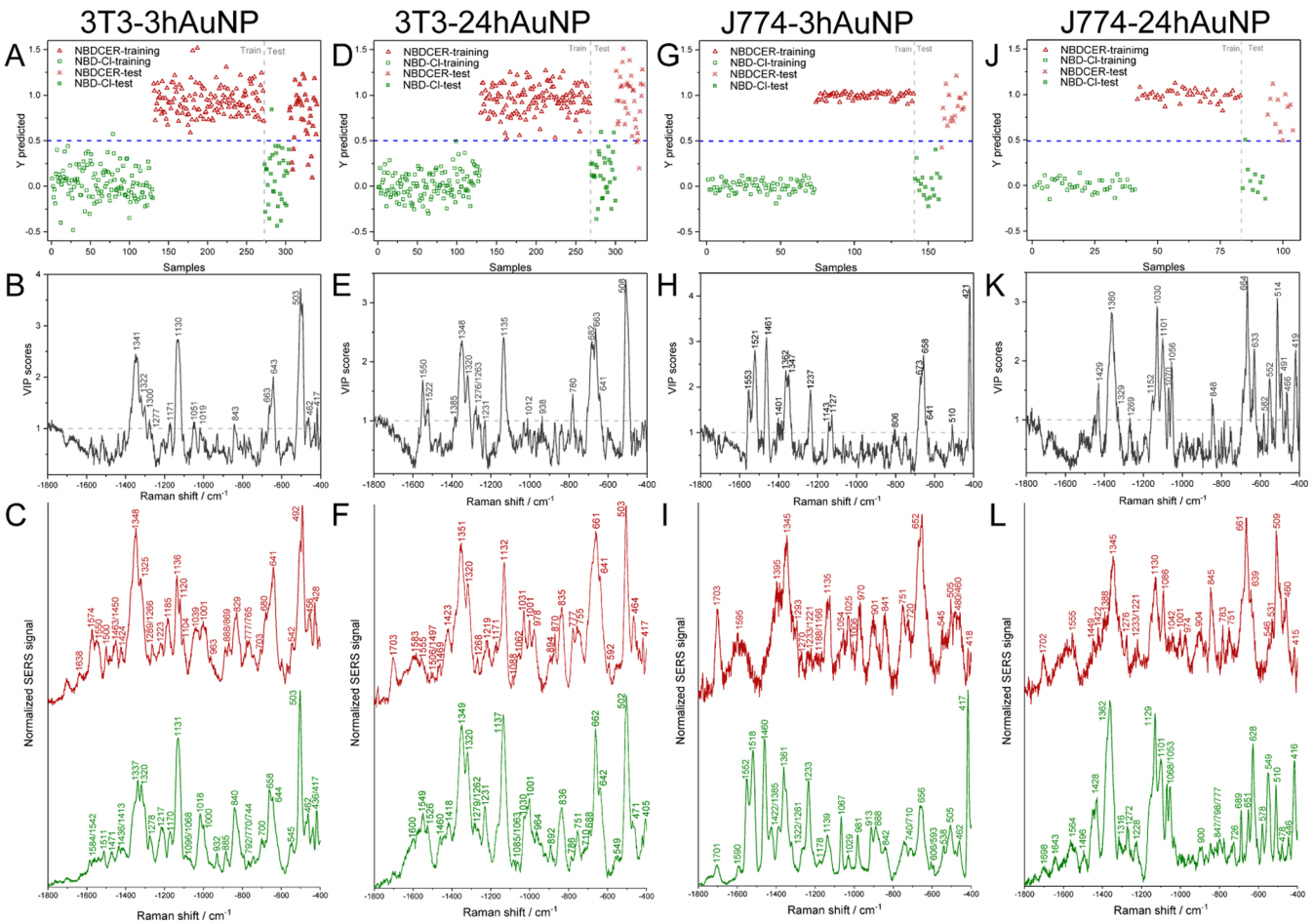

Figure 5. Predictions of the samples (top row) and variable importance in projection (VIP) scores (second row) of the PLS-DA models for discriminating cells of the cell lines 3T3 and J774 treated by NBDCER (red triangles) and NBD-Cl (green squares) after incubation with gold nanoparticles for (A, B, G, H) 3 h and (D, E, J, K) 24 h. In each group, PLS-DA models were trained by 80% of the data (marked as hollow shapes) and tested by the remaining 20% of the data (marked as crossed shapes). Samples placed above the threshold (top row, dashed blue line) are predicted as cells treated by NBDCER, and those below are assigned to cells treated by NBD-Cl. (C, F, I, L) Corresponding average SERS spectra were calculated for cells treated by NBDCER (bottom row, red traces) and NBD-Cl (bottom row, green traces). Excitation wavelength: 785 nm. Excitation intensity: 3.5×10^5 W cm^{-2}. Acquisition time: 1 s.

that the uptake of NBDCER and NBD-Cl may affect endosome maturation and concomitant protein composition, even in a short incubation time.

In the J774 macrophage cells, the control groups of both SERS probe incubation times show high resemblance, especially with respect to the signals assigned to proteins, in agreement with the very different processing of the SERS nanoprobes compared to the fibroblast cells (compare Figure 3I,L with Figure 3C,F). This is in agreement with the results from earlier work.[45] The treatment of the cells with NBDCER and NBD-Cl induced great spectral variance and highly specific patterns for both kinds of labels (compare Figure 3G with H and J with K, respectively). The variation is very pronounced for the earlier-stage endosomes (Figure 3G,H) and a bit less obvious in the samples incubated with the SERS probes for 24 h (Figure 3J,K) that were in very late-stage endolysosomes. In the samples that were exposed to NBD-Cl (Figure 3H), signals at 1460 and 1518 cm^{-1} can be observed, indicating the presence of this NBD label in the endolysosomes.[43]

The cells treated with NBDCER exhibit a much higher occurrence of a signal assigned to a C−S vibration at 652 cm^{-1} than other contributions (Figure 3G).[49] Accompanied by the significantly decreased presence of signals assigned to intact S−S disulfide bonds in the region 460−510 cm^{-1},[35,47,49] this suggests the exposure of Cys residues and a potential disruption of disulfide bonds, which may be related to protein structural destabilization.[35,52]

Similar to the signals present in the 3T3 fibroblast samples, also the macrophage cells exposed to NBD-Cl (Figure 3H) result in many spectra with signals of Trp at 417 cm^{-1}, pronounced contributions from an amide II mode at 1233 cm^{-1}, and a decreased occurrence of protein backbone C−C/C-N modes around 1120 cm^{-1} as well as Tyr vibration ∼840 cm^{-1} (compare Figure 3H with I),[17,41,47,48,50,53] suggesting the destabilization of protein structures in the immediate environment of the SERS nanoprobes and/or a changed protein composition in the endolysosome.

The changes in protein structure and composition upon exposure of the macrophage cells to NBD-Cl in less mature endosomal structures (Figure 3H) are also found in cells containing more very late-stage endolysosomes (Figure 3K), here mainly displayed by abundant signals of amide III at 1272 cm^{-1}, the disulfide S−S band at 549 cm^{-1} and C−S signal at 628 cm^{-1},[20,47−50] suggesting an increased exposure of the proteins to the nanoprobe surface. Moreover, signals of Trp at 416 cm^{-1} occurred more frequently,[35,47,48] while both Phe and

https://doi.org/10.1021/acs.jpcc.4c05260
J. Phys. Chem. C 2024, 128, 19722−19735

Tyr signals are absent (Figure 3K).[17,47,50,53] In the predominately late-stage endolysosomes of macrophage samples exposed to NBDCER (Figure 3J), the spectra show many contributions from lipids in addition to the signals assigned to proteins, e.g., at 1449, 1086, 805, and 783 cm^{-1}.[17,18,35,40,47] This is also the case in the cells treated by NBD-Cl (Figure 3K), albeit here other lipid bands are found, including bands assigned to deformation mode of CH_2 groups at 1428 and 1362 cm^{-1}, C−C stretching modes at 1101 and 1068 cm^{-1}, and the lipid ester O−P−O stretching mode at 798 cm^{-1}.[17,18,35,40,47,50,51,54]

Multivariate Classification Based on Different Endolysosomal Composition upon NBDCER and NBD-Cl Exposure. Principal component analysis (PCA) was used to assess the spectral variance within and between the different data sets and to further identify major spectral patterns that are characteristic of the treatment of the two cell types with the two NBD-based labels. Analyses were done with spectra from one cell line and the same gold nanoparticle incubation conditions, corresponding to the columns shown in Figure 3, and their results are shown in Supporting Figure S4. The low variation that is covered even by the first principal components is in good agreement with the high inherent variability and fluctuation of SERS data from complex cellular systems that have been reported before.[48] When using the spectral range of 400−1800 cm^{-1}, several of the groups of data sets show overlap in the scores plots (Figure S4), due to a large heterogeneity within each data set. The spectra obtained from NBDCER labeled J774 macrophage cells are very distinct from the other data, with variance determined by the spectral features discussed above and in good agreement with the more prominent differences in the bands assigned to proteins (Figures 3G and S4E,F) and to lipids (Figures 3J and S4G,H) in earlier and later-stage endolysosomes, respectively. The NBD signals (1519 and 1459 cm^{-1})[43] in the loadings of PC1 and PC2 that separate NBDCER and NBD-Cl treated cells from the controls, respectively, clearly indicate the presence of the labels in the earlier-stage endolysosomes of the J774 macrophages (Figure S4E,F).

While many of the spectra of the NBD-labeled cells are different from those of the respective control groups, the data from endolysosomes of cells exposed to NBDCER and NBD-Cl differ from one another (Figures 3 and S4). Partial least-squares-discriminant analysis (PLS-DA) was conducted to identify the differences between the four data sets from the cells treated with the two different NBD labels. PLS-DA is a supervised multivariate technique that we use here to classify the spectra based on their known origin from a particular sample. In each group of samples, that is, the spectra from the same cell type and SERS probe incubation of cells exposed to NBDCER and those exposed to NBD-Cl, a discriminant model with 10 latent variables was developed. Table 1 shows the classification results as assessed based on cross-validation of the training data as well as on the classification of an independent test set. The prediction performance of the PLS-DA models is visualized in Figure 5 (top row). The performance of the PLS-DA model to identify unknown spectra from earlier-stage endolysosomes of 3T3 cells labeled with NBDCER was found to be the lowest (Table 1, first line, second column).

In order to identify the spectral variables contributing to the variance between the cells exposed to the two different NBD labels, we determined the variable importance in projection (VIP) score and selected those signals with values greater than 1 (Figure 5B,E,H,K).[54,55] Overall, the qualitative differences indicated in the VIP score plots of the data sets (Figure 5B,E,H,K) agree well with the differences regarding lipid and protein composition found in the frequency of occurrence plots discussed in detail above (Figure 3) and the loadings of the first principal components (Supporting Information Figure S4). For comparison, Figure 5 also displays the respective average spectra of each data set (Figure 5C,F,I,L).

In the earlier-stage endolysosomes of 3T3 fibroblast cells, differences between NBDCER and NBD-Cl treatment include lipid signals at 1171 and 1051 cm^{-1} (Figure 5B).[7,18,40,47,48] In the samples that were incubated longer with the SERS probes and contained a wider range of endolysosomal stages (Figure 5E), differences between the incubation with the different NBD labels arise from amide II and amide III contributions, indicating a changed protein composition.

Similar to the PC loadings in Figure S4F, also the VIP scores indicated that the macrophage J774 cells show differences attributed to the NBD group and amide II, III vibrations (Figure 5H) in the earlier-stage endolysosomes. In agreement with the average spectra in Figure 5I, exposure to NBDCER (Figure 5I, top trace) contributes to this distinction e.g., by the signal of the disulfide C−S band at ∼660 cm^{-1},[17,47−49] and Trp at ∼420 cm^{-1},[35,47,48] featured in the average spectrum of cells with NBD-Cl (Figure 5I, bottom trace), produces a strong variance (Figure 5H). In the J774 samples that have a wider range of endolysosomal stages upon 24 h incubation with the nanoprobes (Figure 5K), the contributions from lipid acyl chains appear stronger and underpin their observation in the PC loadings (Figure S4H). Moreover, the pronounced S−S and C−S vibrational modes at 664, 633, 582, 552, 514, 491, and 466 cm^{-1} are found to be important in the distinction between the two labeling conditions (Figure 5K).[17,35,47−50] Accordingly, spectral signals are found in the average spectrum of the cells incubated with NBD-Cl (Figure 5L, bottom trace). This indicates that NBD-Cl may affect the interaction of the endolysosomal proteins by sulfur-containing amino acid residues differently.

While the presence of the two NBD labels affects the same cell line differently, they may also have a different influence on the two different cell types. PLS-DA was also carried out to assess the spectral variations between the two cell lines when exposed to the same NBD label for 24 h with the SERS probes in the cells (Table S2). As shown in Table S2, the models effectively distinguish between fibroblast 3T3 and macrophage J774 cells in both the training and independent test data sets. The only exception was J774 cells exposed to NBDCER, with a low success rate for the identification of independent test spectra. The VIP scores for the three experiments are shown in Figure S5. When comparing them for NBDCER (Figure S5A) and NBD-Cl (Figure S5B) treated macrophage and fibroblast cells, extra features from lipid skeletal vibrations in the region 1040−1100 cm^{-1}[17,40,42,50,51,53] indicate an altered lipid composition in the endolysosomes of the two cell types, and a different exposure of protein side chains, indicated by important signals at ∼1030, 1005, and ∼420 cm^{-1}.[35,47,48,50,56] Additional differences between 3T3 and J774 cells were found for the amide II protein signals after exposure of the cells to NBD-Cl (Figure S5B). An assessment of differences between unexposed (control) cells of both cell lines was conducted, as well. The VIP scores of the control group (Figure S5C) illustrate that the prominent features to differentiate between

https://doi.org/10.1021/acs.jpcc.4c05260
J. Phys. Chem. C 2024, 128, 19722−19735

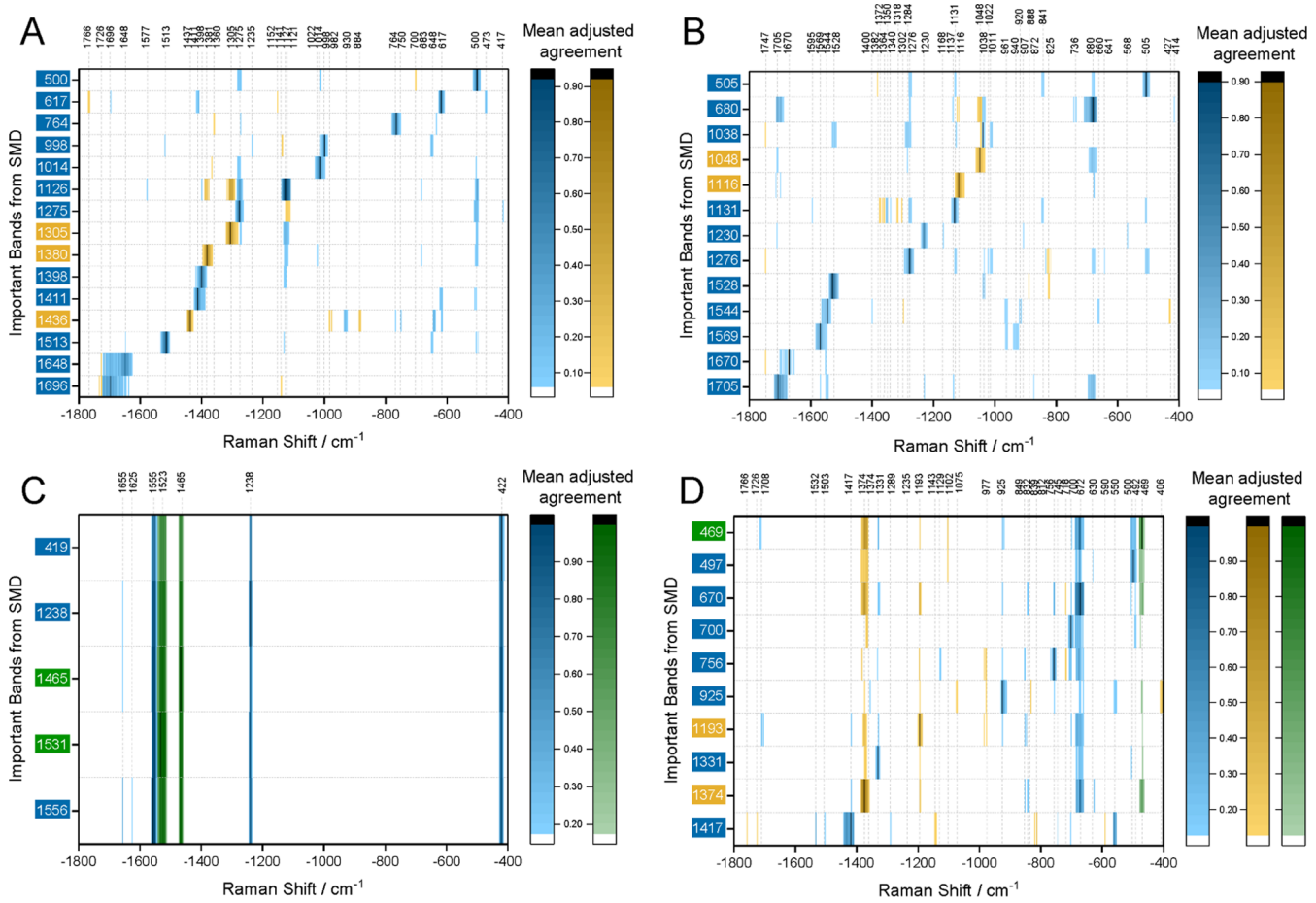

Figure 6. Spectral variables co-occurring with the important bands (left) selected by SMD analysis (cf. Figure S6) of SERS spectra from (A, B) 3T3 and (C, D) J774 cells treated by NBDCER and NBD-Cl after incubation with gold nanoparticles for (A, C) 3 h and (B, D) 24 h. Bands assigned to proteins marked in blue, to lipids in yellow, and to NBD in green.

the two cell lines are mainly attributed to protein backbone, amino acids, and disulfide residues. The great contribution of the bands at 1320 cm^{-1} accompanied by peaks at 1420 and 1042 cm^{-1} indicates distinct lipid environments.[18,20,40,47,48,51] This further supports that the spectral differences between the cells exposed to the different NBD labels and within the controls from both cell lines may be linked to a cell-type-specific response to NBDCER and NBD-Cl.

Random Forest Analysis Points to Different Endolysosomal Responses. Using the same training and test data sets as for PLS-DA, random forest (RF) models were trained for the classification of the data of the cells treated with the different NBD labels. Their classification performances are listed in the last two columns of Table 1. More than 80% of spectra in the independent test data sets were classified correctly. Overall, the results of the random forest classification are comparable to those based on PLS-DA (Table 1). Classification is attained according to the effects of the two NBD labels in the two cell lines and in experiments that use two incubation times with the SERS probes, yielding four classification experiments.

Since it is possible to discriminate between the different spectral classes that represent the different samples with a high success rate (Table 1), surrogate minimal depth (SMD) can be usefully applied here to identify the spectral variables used by the RF model.[16] In this way, those spectral features that are needed to attain classification can be identified. More importantly, the utilization of SMD can identify co-occurring spectral features and thereby help to analyze the interaction of different molecules. The selection of important bands utilizing SMD importance for the four classification experiments is shown in Figure S6. In addition to several features from proteins and lipids that were already identified by the VIP score of PLS-DA above (cf. Figure 5B,E,H), RF-SMD reveals several more differences, including other signals from the same molecules (Figure S6). This confirms the assignment of smaller differences of protein and lipid signals in the spectral classes and the conclusions that changes in their composition and interaction differ upon uptake of NBDCER and NBD-Cl into the cells.

In order to quantify the relationship between the features, the parameter mean adjusted agreement (MAA) is also determined by SMD. This parameter evaluates how well features can replace each other in the RF and can be considered a supervised correlation coefficient. The relationship of all pairwise combinations of spectral variables by the MAA results in large data matrices that can be used to infer the co-occurrence of signals and on colocalization of molecular groups, molecules, and/or their interactions. Figure 6A–D shows the relation parameters of all spectral variables with the important bands identified in Figure S6, corresponding to each of the data groups (each cell line and SERS probe incubation time), highlighting their assignments to different molecular classes through different colors (blue markings, protein; yellow

https://doi.org/10.1021/acs.jpcc.4c05260
J. Phys. Chem. C 2024, 128, 19722−19735

markings, lipid; green markings, NBD group). The result shown in Supporting Figures S7−S10 displays the full MAA matrices for each of the RF models shown in Figure 6. A higher MAA of a variable indicates its closer relation to the selected important bands (compare the color scale/shade within each of the Supporting Figures S7−S10).[21]

In the fibroblast cells where probing occurred in endolysosomes of earlier stages (Figure 6A), the signals of the C−C/C-N vibrational modes of protein chain ∼1130 cm^{-1} and of their disulfide bonds at 683 and 500 cm^{-1} are related to the bands assigned to deformations of lipid CH_2 and CH_3 groups at 1305 and 1380 cm^{-1}.[17,40,47,48,50,57] Considering that these signals can be associated with an interaction of the SERS probes with lipid tails and the protein backbone, the differences between the NBDCER and NBD-Cl treatment are likely in probing different lysosomal proteins and lipids that undergo varying degradation depending on the NBD label to which they are exposed to. In agreement with this, signals of specific protein side chains, e.g., at 930, 764, and 750 cm^{-1} and 617 cm^{-1}, attributed to Pro, Trp, and Phe co-occur with lipid alkyl group deformations at 1438 cm^{-1} that are altered when a packed organization of lipid membranes was probed[17,18,47,48,57] (Figure 6A) and suggests that NBDCER and NBD-Cl may differently affect the exposition of amino acid residues adjacent to organized lipid membranes. When a wide range of endolysosomal stages, including very late-stage lysosomes, are probed in the 3T3 cells (Figure 6B), the protein structure-sensitive amide I vibrations ∼1700 cm^{-1} and a C−S vibration at 675 cm^{-1} co-occur with a signal from the C−C stretching of lipid hydrocarbon chains at 1117 and 1048 cm^{-1}.[17,35,40,47,50,51,53,57] This is a further indicator that the integrity of membrane proteins and the nearby lipid membranes may be influenced to varying extents when NBDCER and NBD-Cl are present in the cells.

The J774 cells exhibited a more sparse variable selection, but the less selected variables showed strong relations with other variables (Figure 6C,D). Particularly, the spectral features that were found to be related to important bands can be assigned to proteins (Figure 6, blue markings), lipids (Figure 6, yellow markings), and NBD (Figure 6, green markings), respectively. When comparing the cell lines 3T3 and J774 for the same SERS probe incubation time of 24 h (compare Figure 6B,6D), the related variables in the RF model of the J774 cells contain more signals that can be assigned to lipid vibrations. Interestingly, also in this analysis, the signals of lipids in J774 are often related to bands that can be directly assigned to NBD. NBD signals were also found in the J774 spectra analyzed in Figure 3, in the PLS-DA VIP scores (Figure 5H,K) and were selected by the surrogate minimal depth (Figure S6C,D, *y*-axis in Figure 6C,D). Figure 6D shows the simultaneous presence of lipid CH_2/CH_3 group deformation modes, vibrations of the phosphate ester bond, protein C−S stretching modes, and the NBD vibrations at 1374, 1193, 670 and 469 cm^{-1}.[40,43,47,48,50] This indicates that free NBD-Cl in J774 is likely to react with Cys residues of proteins near membranes that are rich in phospholipids. The observation of NBD signals in the endolysosomes of J774 but not of 3T3 cells could be related to the specialized functions of macrophages that are highly active in phagocytosis and endocytosis.[58] The cells were exposed to NBD-Cl for a short period of 20 min (Scheme 1), during which the fibroblast cells may not take up and process the external molecules in lysosomes as efficiently as macrophage cells do. In the endolysosomes, NBD-Cl is highly reactive toward nucleophiles, particularly amines and thiols, which are prevalent functional groups in proteins and peptides.[14] Its interaction with numerous proteins within the endolysosomes of the macrophage cells would also facilitate their interaction with the SERS nanoprobes and make them visible in the spectra.

In the RF model of J774 macrophage long-incubation time endolysosomes (Figure 6D), the presence of phosphate and choline groups at 832 and 718 cm^{-1}, respectively, is also associated with vibrations of Pro, Trp, and a C−S stretching mode at 924, 756, and 670 cm^{-1}, respectively, of proteins.[18,20,47,48,50] This may indicate a slight temporary increase of sphingomyelin and choline in the lysosomes that is a possible consequence of a feedback regulation against overabundant ceramide that entered the cells with the NBDCER label.[15,59] Similar to the observations made in the 3T3 fibroblast cell line, spectral contributions by the Tyr, Phe, and disulfide S−S vibrations[17,35,47−49] co-occurring with above phospholipid signals also suggests that proteins in the proximity of the phosphate-rich membranes may alter their structure differently in the presence of NBDCER and NBD-Cl.

Interestingly, the signals of phosphoinositide at 590 and 406 cm^{-1} as important bands were found to be related to those of amino acid carboxylate groups at 1417 cm^{-1} and a Pro C−C vibration at 924 cm^{-1}, respectively, along with bands ascribed to protein amide modes, Trp, disulfide, lipid C−C, and phosphate vibrations[17,47−51,53] (Figure 6D). It was reported recently that the generation of phosphoinositide could be stimulated by the permeabilization of the lysosomal membrane and that it could attract specific complements of functional proteins to membranes in order to support lysosomal membrane repair.[60] NBD-Cl can inhibit nicotinamide nucleotide transhydrogenase activity and mitochondrial respiratory function, causing lower NADPH supply and higher sensitivity toward cell death that is induced by reactive oxygen species[61] that may destabilize the lysosomal membranes.[62] Moreover, the phosphoinositide-3-kinase to produce phosphatidylinositol 3,4-bisphosphate, which locates at endosome membranes,[63] could be activated by C6-ceramide.[64] The data reported here suggest that we probe such an accumulation of proteins at the endolysosomal membranes by the attraction of phosphoinositide as a consequence of excessive NBDCER and NBD-Cl. In the earlier-stage endolysosomes in the macrophage cell lines, the relationships among signals of amide vibrations, Trp, and NBD, as indicated in Figure 6C imply that the colocalization of unfolded proteins and NBD-Cl molecules could be an important indicator of the particular action of the reactive NBD-Cl.[35,43,47,48] Overall, we conclude that the exposure of the cells to NBDCER and NBD-Cl leads to subtle and reproducible changes of protein environment as well as of the surrounding membrane region in endolysosomes of different maturation stages.

Observed Effects of NBD Labels on Cellular Biochemistry can be Related to Their Uptake and Intracellular Processing. The SERS spectra obtained from the cellular models mainly probe the molecular composition and structure of the endolysosomes. Compared to SERS spectra from the control groups, the spectral features of NBD-Cl exposed cells suggest that the cellular uptake of NBD-Cl could alter the endolysosomal environment differently, with interactions of the NBD group and the SERS probes becoming visible directly when NBD-Cl was taken up by macrophages. In addition to a change in processes in the endolysosomes, these

https://doi.org/10.1021/acs.jpcc.4c05260
J. Phys. Chem. C 2024, 128, 19722−19735

changes are likely the cause of the inhibition of important enzymes by NBD-Cl. Particularly, NBD-Cl has been reported to inhibit Bovine F1-ATPase by covalently reacting with a Tyr residue in the βE subunit of the enzyme, preventing it from adopting a nucleotide-binding state.[9] The availability of ATP can have a significant impact on the activity, e.g., of the V-type ATPase that is responsible for lysosome acidification.[65,66] Moreover, the toxicity of NBD-Cl was shown at concentrations that were partially effective in inhibiting enzyme activities and led to typical apoptosis features and a significant decrease in viability.[67] Biochemical changes in endolysosomes under NBD-Cl treatment are also possibly associated with mitochondrial NADPH decline, which can disrupt cellular homeostasis and apoptosis.

Upon addition of NBDCER to cells, no NBD signals were observed in the SERS spectra of the endolysosomes, in agreement with NBDCER shown to stain the Golgi complex and to translocate to the plasma membrane of living cells.[2,15] However, the comparison of the spectral signals from these samples with those of the control group also revealed changes of protein and lipid structure and composition, suggesting that the uptake of NBDCER into the Golgi may indirectly affect the biochemical composition of the endolysosomes. This observation could be related to the action of exogenous C16 ceramide as a potent inductor of apoptosis,[68] as shown by reduced cell viability in coronary artery endothelial cells.[68] Although no apparent visual signs of apoptosis were observed in the fibroblast or macrophage cells exposed to NBDCER (Figure 2B,C), we assume that external ceramide at a concentration of 5 μM, labeled with NBD, could lead to apoptosis-related metabolic activities that could result in the observed changes in the endolysosomal composition in those cells that were treated with NBDCER.

With a number of functional proteins in phospholipid bilayer membranes and in their proximity, extracellular material and intracellular components, including proteins and lipids, are delivered into lysosomes and undergo degradation.[69] Notably, vibrational bands attributed to the NBD group were identified as important variables in the differentiation of macrophage cells exposed to the two different NBD labels. They were found to be related to proteins that reveal disulfide bonds. The data support our hypothesis that NBD-Cl could label biomolecules through thiol and amine functions and that it is partially phagocytosed into endolysosomes by macrophages. In agreement with the known processing and accumulation of NBDCER in the Golgi, outside the endolysosomal system, SMD analysis did not indicate the presence of additional ceramide in endolysosomes in both fibroblasts and macrophages.

CONCLUSIONS

We investigated the biochemical effects associated with the presence of the two NBD labels, NBD-Cl and NBDCER, on cellular biochemistry by probing the molecular composition and interaction in endolysosomes of two different cell lines using SERS. Both molecules, NBD-Cl and NBDCER, exhibit strong and distinct SERS spectra when studied in their pure form using gold nanoparticles as SERS substrates. The spectral features attributed to the vibrational modes of the NBD group in the spectrum of NBDCER indicate that the label group is detectable based on its vibrational spectrum.

The qualitative assessment of spectra from fibroblast and macrophage cells clearly shows differences in the composition and interaction in the endolysosomal system between cells exposed to both NBD labels and the corresponding controls. The differences vary for the cell lines and the incubation conditions.

While NBD-Cl can distribute evenly across different cellular compartments and label different classes of molecules, NBDCER is known to accumulate primarily in the Golgi system. The presence of both types of labels induces changes in the endolysosomal composition. In fibroblast cells, no signals of the NBD moiety are found in the spectra.

In order to explore the "hidden" contributions of the NBD group among the dominant spectral signals of the other components in the endolysosomal compartment that were revealed in a statistical analysis and to elucidate the molecular interactions and connections between the different endolysosomal constituents further, SMD was applied. Specifically, the differences between the molecular compositions with the two different NBD labels were studied in RF models. The co-occurrence of proteins and lipids is consistent with the structural complexity and functional roles of the endolysosomes and known potential effects that NBD labels can have, as reported in work with molecular and cell biological approaches in other cell lines. The differences of the spectral features reveal that the presence of the label NBD, either as NBD-Cl or conjugated with ceramide, has different physiological effects within eukaryotic cells, specifically regarding an altered protein composition and interactions in the endolysosomal system.

In conclusion, these results demonstrate the potential of SERS with gold nanoparticles to probe the intracellular physiological processing of NBD. The molecule has an impact on the composition and interaction of molecules other than the label moiety itself, which can be characterized by SERS. The integration of the local spectroscopic probing and a machine learning approach that offers an identification of classifiers, here, spectral signals of interacting molecular species, reveals the colocalization of molecules and helps to understand the effects of external molecules such as drugs and labels on cellular compartments in vivo. This will clearly apply as well to nonbiological molecule−nanostructure and molecule−molecule interactions that can be elucidated from SERS spectra.

ASSOCIATED CONTENT

Supporting Information

The Supporting Information is available free of charge at https://pubs.acs.org/doi/10.1021/acs.jpcc.4c05260.

Molecular structures of NBD-Cl and NBDCER, characterization of liposomes containing NBDCER, assignment table of bands in the SERS spectra, variability of individual SERS spectra from cells incubated with gold nanoparticles as SERS probes, results of principal component analyses (PCA) of SERS spectra from fibroblast and macrophage cells treated with NBD-Cl and NBDCER, results of partial least-squares-discriminant analysis (PLS-DA) of SERS spectra from cells with the same treatments, and selections of important bands and relation analysis of all spectral variables by the importance and relation parameter of SMD, respectively (PDF)

https://doi.org/10.1021/acs.jpcc.4c05260
J. Phys. Chem. C 2024, 128, 19722−19735

AUTHOR INFORMATION

Corresponding Author

Janina Kneipp − *Department of Chemistry, Humboldt-Universität zu Berlin, 12489 Berlin, Germany;* orcid.org/0000-0001-8542-6331; Email: janina.kneipp@chemie.hu-berlin.de

Authors

Yiqing Feng − *Department of Chemistry, Humboldt-Universität zu Berlin, 12489 Berlin, Germany; Einstein Center of Catalysis (EC2/BIG-NSE), Technische Universität Berlin, 10587 Berlin, Germany*

Florian Gärber − *Hamburg School of Food Science, Department of Chemistry, Universität Hamburg, 20146 Hamburg, Germany*

Essa M. Saied − *Department of Chemistry, Humboldt-Universität zu Berlin, 12489 Berlin, Germany*

Cecilia Spedalieri − *Department of Chemistry, Humboldt-Universität zu Berlin, 12489 Berlin, Germany;* orcid.org/0000-0001-7480-0404

Zdravko Kochovski − *Helmholtz-Zentrum Berlin für Materialien und Energie, Institute of Electrochemical Energy Storage, 14109 Berlin, Germany;* orcid.org/0000-0001-8375-0365

Stephan Werner − *Helmholtz-Zentrum Berlin für Materialien und Energie, Department X-ray Microscopy, 12489 Berlin, Germany*

Christoph Pratsch − *Helmholtz-Zentrum Berlin für Materialien und Energie, Department X-ray Microscopy, 12489 Berlin, Germany*

Christoph Arenz − *Department of Chemistry, Humboldt-Universität zu Berlin, 12489 Berlin, Germany*

Stephan Seifert − *Hamburg School of Food Science, Department of Chemistry, Universität Hamburg, 20146 Hamburg, Germany*

Complete contact information is available at: https://pubs.acs.org/10.1021/acs.jpcc.4c05260

Author Contributions

The manuscript was written through contributions of all authors. All authors have given approval to the final version of the manuscript.

Notes

The authors declare no competing financial interest.

ACKNOWLEDGMENTS

The authors thank Jan Simke at the Center for Electron Microscopy (ZELMI), TU Berlin, for TEM experiments, Lars Dannenberg (HU) for the synthesis of the gold nanoparticles, and Prof. Yan Lu at the Joint Lab for Structural Research at the Integrative Research Institute for the Sciences (IRIS Adlershof) for use of the cryo-EM facility. The provision of beamtime at beamline U41-PGM1-XM of HZB-BESSY II, Berlin, is gratefully acknowledged. Y.F. acknowledges funding from the Einstein Center of Catalysis/Berlin International School of Natural Sciences and Engineering (EC2/BIG-NSE). Y.F. and C.S. were supported by Germany's Excellence Strategy (EXC 2008−390540038−UniSysCat). J.K. and S.S. acknowledge funding by Deutsche Forschungsgemeinschaft (DFG) grant 511107129.

REFERENCES

(1) Ghosh, P. B.; Whitehouse, M. W. 7-Chloro-4-Nitrobenzo-2-Oxa-1,3-Diazole: A New Fluorigenic Reagent for Amino Acids and Other Amines. *Biochem. J.* **1968**, *108*, 155−156.

(2) Pagano, R. E.; Sleight, R. G. Defining Lipid Transport Pathways in Animal Cells. *Science* **1985**, *229*, 1051−1057.

(3) Kappe, C.; Mohamed, Z. H.; Naser, E.; Carpinteiro, A.; Arenz, C. A Novel Visible Range FRET Probe for Monitoring Acid Sphingomyelinase Activity in Living Cells. *Chem. - Eur. J.* **2020**, *26*, 5780−5783.

(4) Bernal-Perez, L. F.; Prokai, L.; Ryu, Y. Selective N-Terminal Fluorescent Labeling of Proteins Using 4-Chloro-7-Nitrobenzofurazan: A Method to Distinguish Protein N-Terminal Acetylation. *Anal. Biochem.* **2012**, *428*, 13−15.

(5) Lavis, L. D.; Raines, R. T. Bright Ideas for Chemical Biology. *ACS Chem. Biol.* **2008**, *3*, 142−155.

(6) Jenkinson, D. R.; Cadby, A. J.; Jones, S. The Synthesis and Photophysical Analysis of a Series of 4-Nitrobenzochalcogenadiazoles for Super-Resolution Microscopy. *Chem. - Eur. J.* **2017**, *23*, 12585−12592.

(7) Terrier, F.; Mokhtari, M.; Goumont, R.; Hallé, J.-C.; Buncel, E. High Brønsted B_{nuc} Values in S_nar Displacement. An Indicator of the SET Pathway? *Org. Biomol. Chem.* **2003**, *1*, 1757−1763.

(8) Ellis, H. R.; Poole, L. B. Novel Application of 7-Chloro-4-Nitrobenzo-2-Oxa-1,3-Diazole to Identify Cysteine Sulfenic Acid in the AhpC Component of Alkyl Hydroperoxide Reductase. *Biochemistry* **1997**, *36*, 15013−15018.

(9) Orriss, G. L.; Leslie, A. G.; Braig, K.; Walker, J. E. Bovine F1-ATPase Covalently Inhibited with 4-Chloro-7-Nitrobenzofurazan: The Structure Provides Further Support for a Rotary Catalytic Mechanism. *Structure* **1998**, *6*, 831−837.

(10) Fu, R. C.; Liu, X. F.; Chen, S. Inhibition of Monoamine Oxidase by 7-Chloro-4-Nitrobenzofurazan. *J. Neurochem.* **1990**, *55*, 813−818.

(11) Chander, A. Dicyclohexylcarbodiimide and Vanadate Sensitive ATPase of Lung Lamellar Bodies. *Biochim. Biophys. Acta, Lipids Lipid Metab.* **1992**, *1123*, 198−206.

(12) Pagano, R. E.; Martin, O. C. A Series of Fluorescent N-Acylsphingosines: Synthesis, Physical Properties, and Studies in Cultured Cells. *Biochemistry* **1988**, *27*, 4439−4445.

(13) Hannun, Y. A.; Obeid, L. M. The Ceramide-Centric Universe of Lipid-Mediated Cell Regulation: Stress Encounters of the Lipid Kind. *J. Biol. Chem.* **2002**, *277*, 25847−25850.

(14) Chattopadhyay, A. Chemistry and Biology of N-(7-Nitrobenz-2-Oxa-1,3-Diazol-4-yl)-Labeled Lipids - Fluorescent Probes of Biological and Model Membranes. *Chem. Phys. Lipids* **1990**, *53*, 1−15.

(15) Lipsky, N. G.; Pagano, R. E. Sphingolipid Metabolism in Cultured Fibroblasts: Microscopic and Biochemical Studies Employing a Fluorescent Ceramide Analogue. *Proc. Natl. Acad. Sci. U.S.A.* **1983**, *80*, 2608−2612.

(16) Kneipp, J.; Seifert, S.; Gärber, F. SERS Microscopy as a Tool for Comprehensive Biochemical Characterization in Complex Samples. *Chem. Soc. Rev.* **2024**, *53*, 7641−7656.

(17) Živanović, V.; Seifert, S.; Drescher, D.; Schrade, P.; Werner, S.; Guttmann, P.; Szekeres, G. P.; Bachmann, S.; Schneider, G.; Arenz, C.; Kneipp, J. Optical Nanosensing of Lipid Accumulation Due to Enzyme Inhibition in Live Cells. *ACS Nano* **2019**, *13*, 9363−9375.

(18) Feng, Y.; Kochovski, Z.; Arenz, C.; Lu, Y.; Kneipp, J. Structure and Interaction of Ceramide-Containing Liposomes with Gold Nanoparticles as Characterized by SERS and Cryo-EM. *J. Phys. Chem. C* **2022**, *126*, 13237−13246.

(19) Živanović, V.; Kochovski, Z.; Arenz, C.; Lu, Y.; Kneipp, J. SERS and Cryo-EM Directly Reveal Different Liposome Structures During Interaction with Gold Nanoparticles. *J. Phys. Chem. Lett.* **2018**, *9*, 6767−6772.

(20) Živanović, V.; Milewska, A.; Leosson, K.; Kneipp, J. Molecular Structure and Interactions of Lipids in the Outer Membrane of Living Cells Based on Surface-Enhanced Raman Scattering and Liposome Models. *Anal. Chem.* **2021**, *93*, 10106−10113.

(21) Seifert, S.; Gundlach, S.; Szymczak, S. Surrogate Minimal Depth as an Importance Measure for Variables in Random Forests. *Bioinformatics* **2019**, *35*, 3663−3671.
(22) Szekeres, G. P.; Kneipp, J. Different Binding Sites of Serum Albumins in the Protein Corona of Gold Nanoparticles. *Analyst* **2018**, *143*, 6061−6068.
(23) Lösel, H.; Arndt, M.; Wenck, S.; Hansen, L.; Oberpottkamp, M.; Seifert, S.; Fischer, M. Exploring the Potential of High-Resolution Lc-Ms in Combination with Ion Mobility Separation and Surrogate Minimal Depth for Enhanced Almond Origin Authentication. *Talanta* **2024**, *271*, No. 125598.
(24) Wenck, S.; Mix, T.; Fischer, M.; Hackl, T.; Seifert, S. Opening the Random Forest Black Box of 1H NMR Metabolomics Data by the Exploitation of Surrogate Variables. *Metabolites* **2023**, *13*, No. 1075.
(25) Lösel, H.; Brockelt, J.; Gärber, F.; Teipel, J.; Kuballa, T.; Seifert, S.; Fischer, M. Comparative Analysis of LC-ESI-IM-qToF-MS and FT-NIR Spectroscopy Approaches for the Authentication of Organic and Conventional Eggs. *Metabolites* **2023**, *13*, No. 882.
(26) Rohmann, N.; Sturmer, P.; Geisler, C.; Schlicht, K.; Knappe, C.; Hartmann, K.; Turk, K.; Hollstein, T.; Beckmann, A.; Seoudy, A. K.; et al. Effects of Lifestyle and Associated Diseases on Serum CC16 Suggest Complex Interactions among Metabolism, Heart and Lungs. *J. Adv. Res.* **2024**, *59*, 161−171.
(27) Shakiba, N.; Gerdes, A.; Holz, N.; Wenck, S.; Bachmann, R.; Schneider, T.; Seifert, S.; Fischer, M.; Hackl, T. Determination of the Geographical Origin of Hazelnuts (*Corylus Avellana* L.) by near-Infrared Spectroscopy (NIR) and a Low-Level Fusion with Nuclear Magnetic Resonance (NMR). *Microchem. J.* **2022**, *174*, No. 107066.
(28) Wenck, S.; Creydt, M.; Hansen, J.; Gärber, F.; Fischer, M.; Seifert, S. Opening the Random Forest Black Box of the Metabolome by the Application of Surrogate Minimal Depth. *Metabolites* **2022**, *12*, No. 5.
(29) Seifert, S. Application of Random Forest Based Approaches to Surface-Enhanced Raman Scattering Data. *Sci. Rep.* **2020**, *10*, No. 5436.
(30) Lee, P. C.; Meisel, D. Adsorption and Surface-Enhanced Raman of Dyes on Silver and Gold Sols. *J. Phys. Chem. A* **1982**, *86*, 3391−3395.
(31) Samaha, D.; Hamdo, H. H.; Cong, X.; Schumacher, F.; Banhart, S.; Aglar, Ö.; Möller, H. M.; Heuer, D.; Kleuser, B.; Saied, E. M.; Arenz, C. Liposomal FRET Assay Identifies Potent Drug-Like Inhibitors of the Ceramide Transport Protein (CERT). *Chem. - Eur. J.* **2020**, *26*, 16616−16621.
(32) Schneider, G.; Guttmann, P.; Heim, S.; Rehbein, S.; Mueller, F.; Nagashima, K.; Heymann, J. B.; Müller, W. G.; McNally, J. G.; Schneider, G.; et al. Three-Dimensional Cellular Ultrastructure Resolved by X-Ray Microscopy. *Nat. Methods* **2010**, *7*, 985−987.
(33) Schindelin, J.; Arganda-Carreras, I.; Frise, E.; Kaynig, V.; Longair, M.; Pietzsch, T.; Preibisch, S.; Rueden, C.; Saalfeld, S.; Schmid, B.; et al. Fiji: An Open-Source Platform for Biological-Image Analysis. *Nat. Methods* **2012**, *9*, 676−682.
(34) Eilers, P. H. C. A Perfect Smoother. *Anal. Chem.* **2003**, *75*, 3631−3636.
(35) Szekeres, G. P.; Werner, S.; Guttmann, P.; Spedalieri, C.; Drescher, D.; Živanović, V.; Montes-Bayón, M.; Bettmer, J.; Kneipp, J. Relating the Composition and Interface Interactions in the Hard Corona of Gold Nanoparticles to the Induced Response Mechanisms in Living Cells. *Nanoscale* **2020**, *12*, 17450−17461.
(36) Ballabio, D.; Consonni, V. Classification Tools in Chemistry. Part 1: Linear Models. PLS-DA. *Anal. Methods* **2013**, *5*, 3790−3798.
(37) Team, R. C.. *R: A Language and Environment for Statistical Computing*; R Foundation for Statistical Computing: Vienna, Austria, 2022; Vol. *2022*.
(38) Wright, M. N.; Ziegler, A. Ranger: A Fast Implementation of Random Forests for High Dimensional Data in C++ and R. *J. Stat. Software* **2017**, *77*, 5753−5771.
(39) Voges, L. F.; Jarren, L. C.; Seifert, S. Exploitation of Surrogate Variables in Random Forests for Unbiased Analysis of Mutual Impact and Importance of Features. *Bioinformatics* **2023**, *39*, No. btad471.
(40) Tfayli, A.; Guillard, E.; Manfait, M.; Baillet-Guffroy, A. Molecular Interactions of Penetration Enhancers within Ceramides Organization: A Raman Spectroscopy Approach. *Analyst* **2012**, *137*, 5002−5010.
(41) Garidel, P.; Folting, B.; Schaller, I.; Kerth, A. The Microstructure of the Stratum Corneum Lipid Barrier: Mid-Infrared Spectroscopic Studies of Hydrated Ceramide:Palmitic Acid:Cholesterol Model Systems. *Biophys. Chem.* **2010**, *150*, 144−156.
(42) Pemberton, J. E.; Chamberlain, J. R. Raman Spectroscopy of Model Membrane Monolayers of Dipalmitoylphosphatidic Acid at the Air−Water Interface Using Surface Enhancement from Buoyant Thin Silver Films. *Biopolymers* **2000**, *57*, 103−116.
(43) Kurt, M.; Babu, P. C.; Sundaraganesan, N.; Cinar, M.; Karabacak, M. Molecular Structure, Vibrational, UV and NBO Analysis of 4-Chloro-7-Nitrobenzofurazan by DFT Calculations. *Spectrochim. Acta, Part A* **2011**, *79*, 1162−1170.
(44) Muniz-Miranda, M.; Del Rosso, T.; Giorgetti, E.; Margheri, G.; Ghini, G.; Cicchi, S. Surface-Enhanced Fluorescence and Surface-Enhanced Raman Scattering of Push−Pull Molecules: Sulfur-Functionalized 4-Amino-7-Nitrobenzofurazan Adsorbed on Ag and Au Nanostructured Substrates. *Anal. Bioanal. Chem.* **2011**, *400*, 361−367.
(45) Drescher, D.; Büchner, T.; Guttmann, P.; Werner, S.; Schneider, G.; Kneipp, J. X-Ray Tomography Shows the Varying Three-Dimensional Morphology of Gold Nanoaggregates in the Cellular Ultrastructure. *Nanoscale Adv.* **2019**, *1*, 2937−2945.
(46) Drescher, D.; Giesen, C.; Traub, H.; Panne, U.; Kneipp, J.; Jakubowski, N. Quantitative Imaging of Gold and Silver Nanoparticles in Single Eukaryotic Cells by Laser Ablation Icp-Ms. *Anal. Chem.* **2012**, *84*, 9684−9688.
(47) Spedalieri, C.; Szekeres, G. P.; Werner, S.; Guttmann, P.; Kneipp, J. Intracellular Optical Probing with Gold Nanostars. *Nanoscale* **2021**, *13*, 968−979.
(48) Szekeres, G. P.; Montes-Bayón, M.; Bettmer, J.; Kneipp, J. Fragmentation of Proteins in the Corona of Gold Nanoparticles as Observed in Live Cell Surface-Enhanced Raman Scattering. *Anal. Chem.* **2020**, *92*, 8553−8560.
(49) López-Tobar, E.; Hernández, B.; Ghomi, M.; Sanchez-Cortes, S. Stability of the Disulfide Bond in Cystine Adsorbed on Silver and Gold Nanoparticles as Evidenced by SERS Data. *J. Phys. Chem. C* **2013**, *117*, 1531−1537.
(50) Movasaghi, Z.; Rehman, S.; Rehman, I. U. Raman Spectroscopy of Biological Tissues. *Appl. Spectrosc. Rev.* **2007**, *42*, 493−541.
(51) Taylor, R. W.; Benz, F.; Sigle, D. O.; Bowman, R. W.; Bao, P.; Roth, J. S.; Heath, G. R.; Evans, S. D.; Baumberg, J. J. Watching Individual Molecules Flex within Lipid Membranes Using SERS. *Sci. Rep.* **2014**, *4*, No. 5940.
(52) Góngora-Benítez, M.; Tulla-Puche, J.; Albericio, F. Multifaceted Roles of Disulfide Bonds. Peptides as Therapeutics. *Chem. Rev.* **2014**, *114*, 901−926.
(53) Parker, F. S. *Applications of Infrared, Raman, and Resonance Raman Spectroscopy in Biochemistry*; Springer Science & Business Media, 1983.
(54) Chong, I.-G.; Jun, C.-H. Performance of Some Variable Selection Methods When Multicollinearity Is Present. *Chemom. Intell. Lab. Syst.* **2005**, *78*, 103−112.
(55) Farrés, M.; Platikanov, S.; Tsakovski, S.; Tauler, R. Comparison of the Variable Importance in Projection (VIP) and of the Selectivity Ratio (SR) Methods for Variable Selection and Interpretation. *J. Chemom.* **2015**, *29*, 528−536.
(56) Notingher, I.; Green, C.; Dyer, C.; Perkins, E.; Hopkins, N.; Lindsay, C.; Hench, L. L. Discrimination between Ricin and Sulphur Mustard Toxicity in Vitro Using Raman Spectroscopy. *J. R. Soc., Interface* **2004**, *1*, 79−90.
(57) Czamara, K.; Majzner, K.; Pacia, M. Z.; Kochan, K.; Kaczor, A.; Baranska, M. Raman Spectroscopy of Lipids: A Review. *J. Raman Spectrosc.* **2015**, *46*, 4−20.
(58) Gordon, S. The Macrophage: Past, Present and Future. *Eur. J. Immunol.* **2007**, *37*, S9−S17.

https://doi.org/10.1021/acs.jpcc.4c05260
J. Phys. Chem. C 2024, 128, 19722−19735

(59) Lee, A. H.; Snider, J. M.; Moorthi, S.; Coant, N.; Trayssac, M.; Canals, D.; Clarke, C. J.; Luberto, C.; Hannun, Y. A. A Comprehensive Measure of Golgi Sphingolipid Flux Using NBD C6-Ceramide: Evaluation of Sphingolipid Inhibitors. *J. Lipid Res.* **2024**, *65*, No. 100584.
(60) Tan, J. X.; Finkel, T. A Phosphoinositide Signalling Pathway Mediates Rapid Lysosomal Repair. *Nature* **2022**, *609*, 815−821.
(61) Sheeran, F. L.; Rydstrom, J.; Shakhparonov, M. I.; Pestov, N. B.; Pepe, S. Diminished Nadph Transhydrogenase Activity and Mitochondrial Redox Regulation in Human Failing Myocardium. *Biochim. Biophys. Acta, Bioenerg.* **2010**, *1797*, 1138−1148.
(62) Johansson, A.-C.; Appelqvist, H.; Nilsson, C.; Kågedal, K.; Roberg, K.; Öllinger, K. Regulation of Apoptosis-Associated Lysosomal Membrane Permeabilization. *Apoptosis* **2010**, *15*, 527−540.
(63) Falkenburger, B. H.; Jensen, J. B.; Dickson, E. J.; Suh, B.-C.; Hille, B. Phosphoinositides: Lipid Regulators of Membrane Proteins. *J. Physiol.* **2010**, *588*, 3179−3185.
(64) Gulbins, E.; Brenner, B.; Koppenhoefer, U.; Linderkamp, O.; Lang, F. Fas or Ceramide Induce Apoptosis by Ras-Regulated Phosphoinositide-3-Kinase Activation. *J. Leukocyte Biol.* **1998**, *63*, 253−263.
(65) Kosmidis, E.; Shuttle, C. G.; Preobraschenski, J.; Ganzella, M.; Johnson, P. J.; Veshaguri, S.; Holmkvist, J.; Møller, M. P.; Marantos, O.; Marcoline, F.; et al. Regulation of the Mammalian-Brain V-ATPase through Ultraslow Mode-Switching. *Nature* **2022**, *611*, 827−834.
(66) Mindell, J. A. Lysosomal Acidification Mechanisms. *Annu. Rev. Physiol.* **2012**, *74*, 69−86.
(67) Bicego, R.; Francisco, A.; Ruas, J. S.; Siqueira-Santos, E. S.; Castilho, R. F. Undesirable Effects of Chemical Inhibitors of $NAD(P)^+$ Transhydrogenase on Mitochondrial Respiratory Function. *Arch. Biochem. Biophys.* **2020**, *692*, No. 108535.
(68) Zietzer, A.; Jahnel, A. L.; Bulic, M.; Gutbrod, K.; Düsing, P.; Hosen, M. R.; Dörmann, P.; Werner, N.; Nickenig, G.; Jansen, F. Activation of Neutral Sphingomyelinase 2 through Hyperglycemia Contributes to Endothelial Apoptosis Via Vesicle-Bound Intercellular Transfer of Ceramides. *Cell. Mol. Life Sci.* **2022**, *79*, No. 48.
(69) Saftig, P.; Klumperman, J. Lysosome Biogenesis and Lysosomal Membrane Proteins: Trafficking Meets Function. *Nat. Rev. Mol. Cell Biol.* **2009**, *10*, 623−635.

https://doi.org/10.1021/acs.jpcc.4c05260
J. Phys. Chem. C 2024, 128, 19722−19735